



RESEARCH ARTICLE

10.1002/2017JC012838

Special Section:

The Southern Ocean Carbon and Climate Observations and Modeling (SOCCOM) Project: Technologies, Methods, and Early Results

Key Points:

- Biogeochemical sensors on profiling floats require careful adjustments for sensor calibration error and drift
- After adjustment, biogeochemical sensor data can approach the accuracy found in large data sets such as GLODAP
- Adjusted sensor data accuracy has relatively little degradation over the many years a profiling float operates

Correspondence to:

K. S. Johnson,
johnson@mbari.org

Citation:

Johnson, K. S., et al. (2017), Biogeochemical sensor performance in the SOCCOM profiling float array, *J. Geophys. Res. Oceans*, 122, 6416–6436, doi:10.1002/2017JC012838.

Received 27 FEB 2017

Accepted 23 JUN 2017

Accepted article online 5 JUL 2017

Published online 18 AUG 2017

© 2017. The Authors.

This is an open access article under the terms of the Creative Commons Attribution-NonCommercial-NoDerivs License, which permits use and distribution in any medium, provided the original work is properly cited, the use is non-commercial and no modifications or adaptations are made.

Biogeochemical sensor performance in the SOCCOM profiling float array

Kenneth S. Johnson¹ , Joshua N. Plant¹ , Luke J. Coletti¹, Hans W. Jannasch¹ , Carole M. Sakamoto¹ , Stephen C. Riser², Dana D. Swift², Nancy L. Williams³ , Emmanuel Boss⁴ , Nils Haëntjens⁴ , Lynne D. Talley⁵ , and Jorge L. Sarmiento⁶

¹Monterey Bay Aquarium Research Institute, Moss Landing, California, USA, ²School of Oceanography, University of Washington, Seattle, Washington, USA, ³College of Earth, Ocean, and Atmospheric Sciences, Oregon State University, Corvallis, Oregon, USA, ⁴School of Marine Sciences, University of Maine, Orono, Maine, USA, ⁵Scripps Institution of Oceanography, University of California, San Diego, La Jolla, California, USA, ⁶Program in Atmospheric and Oceanic Sciences, Princeton University, Princeton, New Jersey, USA

Abstract The Southern Ocean Carbon and Climate Observations and Modeling (SOCCOM) program has begun deploying a large array of biogeochemical sensors on profiling floats in the Southern Ocean. As of February 2016, 86 floats have been deployed. Here the focus is on 56 floats with quality-controlled and adjusted data that have been in the water at least 6 months. The floats carry oxygen, nitrate, pH, chlorophyll fluorescence, and optical backscatter sensors. The raw data generated by these sensors can suffer from inaccurate initial calibrations and from sensor drift over time. Procedures to correct the data are defined. The initial accuracy of the adjusted concentrations is assessed by comparing the corrected data to laboratory measurements made on samples collected by a hydrographic cast with a rosette sampler at the float deployment station. The long-term accuracy of the corrected data is compared to the GLODAPv2 data set whenever a float made a profile within 20 km of a GLODAPv2 station. Based on these assessments, the fleet average oxygen data are accurate to $1 \pm 1\%$, nitrate to within $0.5 \pm 0.5 \mu\text{mol kg}^{-1}$, and pH to 0.005 ± 0.007 , where the error limit is 1 standard deviation of the fleet data. The bio-optical measurements of chlorophyll fluorescence and optical backscatter are used to estimate chlorophyll *a* and particulate organic carbon concentration. The particulate organic carbon concentrations inferred from optical backscatter appear accurate to within 35 mg C m⁻³ or 20%, whichever is larger. Factors affecting the accuracy of the estimated chlorophyll *a* concentrations are evaluated.

Plain Language Summary The ocean science community must move toward greater use of autonomous platforms and sensors if we are to extend our knowledge of the effects of climate driven change within the ocean. Essential to this shift in observing strategies is an understanding of the performance that can be obtained from biogeochemical sensors on platforms deployed for years and the procedures used to process data. This is the subject of the manuscript. We show the performance of oxygen, nitrate, pH, and bio-optical sensors that have been deployed on robotic profiling floats in the Southern Ocean for time periods up to 32 months.

1. Introduction

The Southern Ocean is the primary gateway through which the intermediate, deep, and bottom waters of the ocean interact with the sea surface and thus the atmosphere. As a result, the majority of the oceanic uptake of anthropogenic carbon and heat occur within its domain [Frölicher *et al.*, 2015]. The Southern Ocean also has a profound influence on nutrient resupply from the abyss to the surface, which regulates nutrient availability throughout the world ocean [Sarmiento *et al.*, 2004]. Waters of the Southern Ocean are particularly susceptible to ocean acidification, due to low carbonate ion concentrations, and this may have profound ecosystem impacts [McNeil and Matear, 2008; Bednaršek *et al.*, 2012]. Understanding these connections between the Southern Ocean and the rest of the globe is one of the primary research foci identified by the Scientific Committee for Antarctic Research [Kennicutt and Chown, 2014].

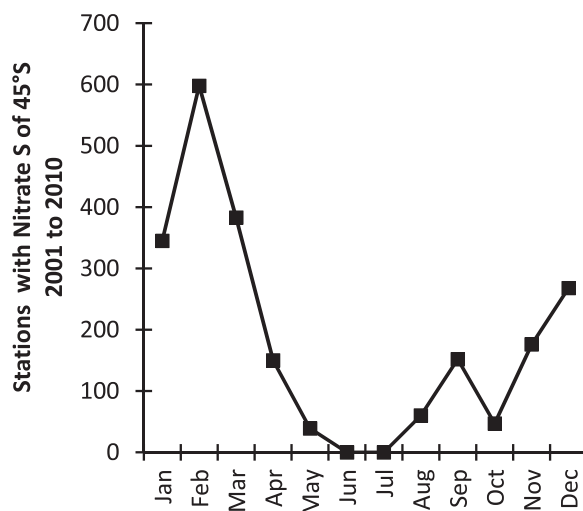


Figure 1. Total number of stations with nitrate data in World Ocean Database 2013, south of 45°S, by month for the period 2001–2010. Source, www.nodc.noaa.gov.

However, the Southern Ocean is also one of the least observed regions of the world ocean due to its geographic remoteness, its extreme weather, and a lack of commercial vessel traffic that might serve as volunteer observing platforms. In particular, during austral winter there can be a nearly complete lack of observations. For example, during the period 2001–2010 there were no oceanographic stations with nitrate data during several months of austral winter (Figure 1). It is clear that new approaches must be utilized if biogeochemical cycles in remote regions like the Southern Ocean are to be observed over complete annual cycles.

Recent advances in technology have the potential to transform our ability to observe and understand the Southern Ocean and its linkages to the global ocean and atmosphere. Modern chemical and biological sensors can operate for multiple years without human intervention [Johnson et al., 2007; Boss et al., 2008].

Profiling floats equipped with these sensors can return multiyear surface and subsurface records of chemical and biological properties throughout complete annual cycles [Körtzinger et al., 2004; Boss et al., 2008; Johnson et al., 2013, 2016a]. This enables studies of ocean biogeochemical processes, including the signal of ocean acidification, ocean deoxygenation, net community production, carbon export, and phytoplankton phenology, in three-dimensional space with a temporal resolution of 5–10 days [Biogeochemical-Argo Planning Group, 2016; Johnson and Claustre, 2016].

The number of chemical profiles collected by profiling floats has increased rapidly in the past 5 years and now exceeds the number of ship-based profiles that reach depths greater than 900 m at any location in the world ocean (Table 1). For example, the Argo database received 6 times more profiles for dissolved oxygen in the year 2016 than the mean annual number of ship-based profiles that reached a depth of 900 m or more in 2000–2010. The discrepancy is likely much greater today because the number of float-based profiles is increasing rapidly, while the number of ship-based profiles is declining precipitously [Johnson et al., 2015]. The average number of ship-based profiles for any parameter received from 2005 to 2015 by NODC declined by tenfold from the values received in the 1980s [Levitus et al., 2013]. Nitrate and pH profiles measured by profiling floats also exceed the number of stations from ships that were added each year to the NODC database (Table 1), even though these sensors are in an early stage of development.

The SOCCOM project is in the process of deploying a large network of profiling floats equipped with oxygen, nitrate, pH, and bio-optical sensors in the Southern Ocean. Determining the impacts of climate processes on carbon flux is a major goal of SOCCOM. The operation of biogeochemical sensors on profiling

floats enables chemical concentrations to be observed over complete annual cycles and through multiple years. In most studies of the Southern Ocean, annual chemical cycles must be compiled from climatologies that are produced from scattered measurements over many years. This obscures many processes such as interannual variability [Lee, 2001; MacCreedy and Quay, 2001]. Only in the Drake Passage are there usually sufficient data to directly examine interannual variability in chemical concentrations [Munro et al., 2014] without

Table 1. Average Number of Ship-Based Oceanographic Profiles per Year From 2000 to 2010 in the World Ocean Database 2013 Which Reach at Least 900 m for the Parameter Indicated, and the Number of Profiles for the Year 2016 Collected by Profiling Floats and Found in the Argo Global Data Assembly Center^a

Parameter	Ship Profiles per Year	Argo Profiles per Year
Oxygen	1,730	11,332
Nitrate	1,231	3,835
pH direct	460	1,862
pH (TA/DIC)	540	
Source	NODC	Argo GDAC

^apH may be measured directly or calculated if both total alkalinity and dissolved inorganic carbon are measured. Both values are shown.

remapping spatially disparate data sets [Takahashi *et al.*, 2014; Landschützer *et al.*, 2016]. The Southern Ocean plays an essential role in ocean uptake of carbon dioxide [Frölicher *et al.*, 2015]. The observations of pH allow the partial pressure of CO₂ (pCO₂) to be estimated over complete annual cycles [Williams *et al.*, 2017] in a region that has few winter observations [Bakker *et al.*, 2016]. This allows the often competing processes of the solubility and biological carbon pumps [Takahashi *et al.*, 2014] to be disentangled and their roles to be more completely understood.

Observing System Simulation Experiments suggest that 200 profiling floats that are randomly distributed south of 30°S with suitable pH sensors could reduce uncertainty in air-sea CO₂ flux to 0.1 PgC yr⁻¹, a factor of 3 or more improvement in current estimates [Majkut *et al.*, 2014]. This estimate of 200 floats has become the target density for the SOCCOM program. A true random distribution is not possible to attain without an excessive amount of ship time, and SOCCOM has essentially no dedicated ship time. The program is dependent on existing US and international research cruises to deploy floats. Further, the 200 float array is being deployed in small annual increments over 6 years and the array will be extremely sparse for much of the program life. The strategy for float deployments is, therefore, to attempt to sample the major regimes and water masses of the Southern Ocean as the array is built. This strategy and the means to accomplish it will be described in an article to appear in the future. To assess sensor accuracy, a profile of water samples was collected immediately preceding each float deployment. This requirement led to a significant collaboration with the International GO-SHIP program [Talley *et al.*, 2016] and deployment from GO-SHIP cruises, which also influenced float deployment locations.

The SOCCOM array is the first basin-scale chemical sensor network that is being operated as an integrated system. The papers in this special issue highlight the potential of such a network to greatly extend our understanding of ocean processes. However, autonomous sensor systems also have limitations. Given the potential of these systems to solve the chronic undersampling that occurs in the Southern Ocean, it is essential to understand the problems that arise when operating these sensors, the processes for correcting data for known biases, and the final quality of the data sets produced by these systems. The chemical sensors used in the SOCCOM program typically suffer from two problems. These are inaccurate initial calibrations, which result from sensor instability during storage and transport before deployment, and subsequent drift or offsets that occur during deployment. Correction for these problems is the main issue in their operation. Solutions to similar problems have been developed by the Argo program to correct for salinity sensor drift [Owens and Wong, 2009] and by the Global Ocean Data Analysis Project (GLODAP) to produce consistent data sets from a collection of hydrographic cruises [Olsen *et al.*, 2016]. Here we examine the procedures that are currently employed in the SOCCOM program to correct the deficiencies in biogeochemical sensors and the properties of the resulting data set. We also consider areas where this process could be improved in the future and provide several suggestions that may improve float data processing.

2. Materials and Methods

2.1. SOCCOM Floats and Biogeochemical Sensors

The SOCCOM program has deployed two types of profiling floats in all regions of the Southern Ocean (Figure 2), including areas with seasonal ice cover. Autonomous Profiling Explorers (APEX) floats using the APF9 controller were assembled at the University of Washington from components purchased from Teledyne/Webb Research. Each of these floats was pressure tested to the full deployment depth before shipping. BGC Navis floats were purchased from Seabird Electronics and used as received after a set of basic operational checks recommended by the manufacturer. Engineers at institutions participating in SOCCOM are most familiar with the APEX floats. They have written the computer code that operates the floats and sensors. They have also developed the pH and nitrate sensors that play a central role in the science program. This familiarity has resulted in a high survival rate for the floats and flexibility in the implementation of the biogeochemical sensors that is not generally available with a fully commercial system. As a result, most of the SOCCOM floats have been of this type, which ensures maximum data return and a rapid response to systematic problems as they are identified. However, these specific systems are not generally made available to the science community outside of SOCCOM. SOCCOM has a programmatic commitment to ensuring that the technology developed by its engineers becomes widely available. The project is, therefore, also working with commercial vendors to ensure that there is an equivalent capability available to the

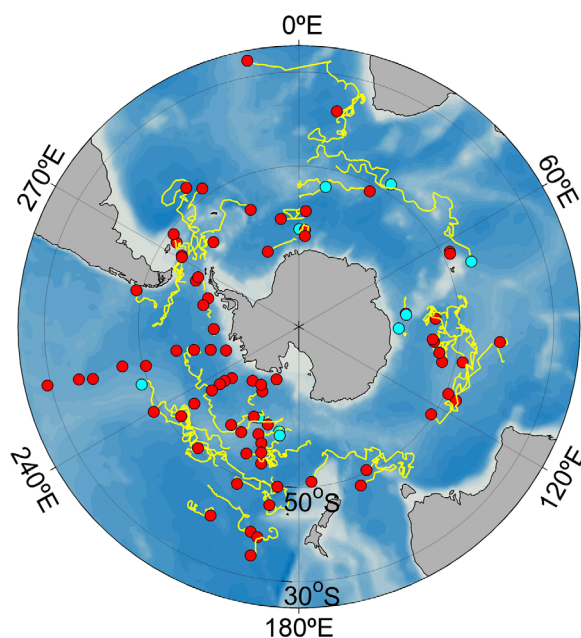


Figure 2. Red dots show location of active SOCCOM floats in mid-February 2017. Trajectories are shown as yellow lines. Blue dots are last location of inactive floats.

community. Most of this effort to date has been focused on Navis floats because of the proximity between the manufacturer and the University of Washington float laboratory. As Navis float capability has evolved, they have been deployed within the SOCCOM array at locations suitable to assess various aspects of their performance.

Both types of floats are capable of about 250 profiles. They follow a standard Argo mission with a profile at 10 day intervals, which should yield lifetimes around 6.5 years before the batteries expire. There is a distinct trade-off between profiling at 10 day intervals and higher frequencies. Ten days provides only coarse resolution for biological processes such as a spring bloom and this could be improved with shorter cycle times. However, reducing the cycle time has a direct impact on float life time and the resulting array size. Cycle times much shorter than 10 days would exhaust batteries in less than 6 years. We have opted for a 10 day cycle time to extend the life of the earliest

SOCCOM floats to the end of the 6 year program. A uniform cycle time is used to ensure adequate sampling in winter, where little data exists for processes such as air-sea CO₂ flux [Williams *et al.*, 2017]. The vertical sampling resolution for the CTD and chemical sensors is summarized for each float type in Table 2. The highest vertical resolution of each float type is a reflection of the capabilities of the float controller and CTD electronics on each platform. On APEX floats, sensor sampling is handled by the float controller and is limited to about 5 m resolution, and is generally lower to save power. In particular, sampling resolution for nitrate is limited by power consumption [Johnson *et al.*, 2013] to about 70 samples on a profile from 2000 m. Samples are taken at the highest resolution in the upper 100 m and at increasingly lower resolution at greater depths. Sensor sampling on Navis floats is handled by the CTD and can proceed at a higher rate, except for nitrate.

The floats park at 1000 m between profiles, following Argo protocol, and then descend to a maximum depth between 1400 and 2000 m before returning the surface. Profile measurements are made on this ascent and transmitted via the Iridium satellite network at the ocean surface before the float descends back to its park depth. Surface time is less than 15 min. All raw data are available in real time. The quality-controlled data stream is initialized within a few months after float deployment when sufficient profiles are available for the adjustment processes described below. The quality-controlled data stream is then produced in real time and corresponds to Argo real-time, adjusted data. All data enters the Argo database as well as a database (SOCCOMViz) maintained by the SOCCOM program.

Table 2. Vertical Sampling Resolution (m) for APEX and Navis Floats Used in the SOCCOM Program

Float Type	APEX	Navis
CTD Z < 1000	2	2
CTD Z > 1000	100	50
Chemistry Z > 1000	100	50
Oxygen Z < 1000	Schedule	2
pH Z < 1000	Schedule	2
Nitrate Z < 1000	Schedule	Schedule
Bio-optics	Schedule	2
<i>Schedule</i>		
Z < 100	5	
100 < Z < 360	10	
360 < Z < 400	20	
400 < Z < 1000	50	

In addition to the traditional Argo T, S, and P sensors (SBE 41CP CTD on APEX and SBE 41N on Navis), the floats are equipped with oxygen, nitrate, and pH chemical sensors, and chlorophyll fluorescence and 700 nm optical backscattering sensors, with a few exceptions. Navis floats also carry a

fluorescent dissolved organic matter (FDOM) sensor or an additional backscattering sensor at 532 nm. The FDOM sensor data are reported using the manufacturer's calibration and no further adjustments are made. The FDOM sensors are not considered further in this paper. Three models of oxygen sensors have been deployed in the SOCCOM program, Aanderaa 3830 and 4330 Optodes and Seabird Electronics SBE 63 Optodes. These are all fluorescence lifetime based sensors, which have been used extensively in ocean studies.

The APEX floats are equipped with In Situ Ultraviolet Spectrophotometer (ISUS) optical nitrate sensors that were built and calibrated at MBARI. The Navis floats carry Submersible Ultraviolet Nitrate Analyzers (SUNA) optical nitrate sensors that were built and calibrated at Satlantic. Both of these sensors operate on the same principle and have many of their optical components in common. The major differences are the layout of the optical cells on each instrument type, and the main ISUS components are internal to the float pressure housing and do not contribute to float volume, while the entire SUNA is mounted outside the float pressure hull and interfaced through an underwater cable. We chose to use ISUS on APEX floats because there are fewer potential failure modes due to an absence of external cables and because the greater volume affects the maximum depth attainable by an APEX float. SBE chose the SUNA because of easier mechanical integration. The UV spectral data were transmitted to shore and nitrate concentrations were calculated according to Argo protocols [Johnson *et al.*, 2016b]. Processing included a pressure coefficient of $-2.6\%/1000$ dbar for the absorptivity of sea salt. The presence of this effect was suggested by Pasqueron de Fommervault *et al.* [2015]. It was subsequently confirmed by laboratory measurements at MBARI. The pressure coefficient was implemented in the calculation of nitrate as described by Johnson *et al.* [2016b, equation (7)].

Deep-Sea DuraFET pH sensors were used to determine pH. These contain an Ion Sensitive Field Effect Transistor proton sensor and a AgCl reference sensor for chloride ion [Johnson *et al.*, 2016a]. The sensors are calibrated to report pH on the total proton scale [Dickson *et al.*, 2007] at in situ temperature and pressure. All pH calibrations follow the procedure described in Johnson *et al.* [2016a]. The pH sensor is sensitive to light and it was placed in the flow stream of the CTD with a black housing to shield it from light.

The raw engineering data from each sensor are processed to state variables such as nitrate and oxygen concentration following Argo procedures [Schmechtig *et al.*, 2015, 2016; Thierry *et al.*, 2016; Johnson *et al.*, 2016b]. Additional procedures for quality control and data adjustment are described below.

Bio-optical data were collected on the float using one of two models of bio-optical sensors. The WET Labs ECO-FLBB AP2 (FLBB hereafter) with a chlorophyll *a* fluorometer (EXcitation/EMission 470/695 nm) and backscatter sensor with a 700 nm light source and centroid scattering angle of $\theta = 142^\circ$ is deployed on APEX floats. The WET Labs MCOMS, which includes a chlorophyll *a* fluorometer (EX/EM 470/695 nm) and a backscatter sensor with a 700 nm light source and a scattering angle $\theta = 150^\circ$, and an FDOM fluorometer (EX/EM 370/460 nm) is deployed on Navis floats. The major difference is the angle of scattering in the back-direction and the illuminated volume, which is larger in the MCOMS. Everything else discussed here pertains to both sensors.

Both the APEX and Navis floats that have been deployed to the south of 50° were equipped with ice avoidance software [Wong and Riser, 2011]. These floats are exposed to water temperatures as low as -1.8°C . All of the sensors used here are capable of operating in these conditions. This has allowed the SOCCOM program to obtain some of the first annual cycles of biogeochemical data within the seasonal ice zone.

2.2. Hydrographic Data

In general, each float deployment occurred at an oceanographic station where water samples were also collected to measure oxygen, nitrate, and pH (or total alkalinity and dissolved inorganic carbon from which pH can be calculated) by standard methods [Hood *et al.*, 2010]. Oxygen was determined by Winkler titration and nitrate by automated analyzer. pH was determined spectrophotometrically with purified dye [Liu *et al.*, 2011]. Values are reported on the total proton scale. Total alkalinity, and dissolved inorganic carbon analyses followed standard methods, including the use of standard reference materials [Dickson *et al.*, 2007].

Water samples were also collected for pigment analysis and particulate organic carbon (POC). A volume of 1 or 2 L was filtered on glass fiber filters (GFF) for each analysis and then stored in liquid nitrogen. The filters for high-performance liquid chromatography pigment analysis (HPLC) were analyzed at either the NASA Goddard Space Flight Center or at CSIRO following the same protocol. Particulate organic carbon was analyzed at the MSI Laboratory at UCSB. The HPLC analysis follows the protocol of Van Heukelem and Thomas

[2001] (further described in *Hooker et al.* [2005]). The total chlorophyll (chl *a*) reported from HPLC corresponds to the sum of divinyl chlorophyll *a*, monovinyl chlorophyll *a*, chlorophyllide *a*, chlorophyll *a* allomers, and chlorophyll *a* epimers.

Pigment and POC samples were limited to depths shallower than 100 m because of a focus on upper ocean processes and because of a concern for biases at low POC concentrations [*Gardner et al.*, 2003]. The filtered POC samples were acidified to remove inorganic carbon. A dry blank (unused filter) was collected at the time of sampling to account for potential contamination between the time the sample was taken and the time of analysis in the lab. The POC extracted from the dry blank was removed from the POC extracted for each sample. A “wet” blank filter to account for the effect of dissolved organic carbon (DOC) adsorption was not taken. For the volume filtered in this work, such blanks typically vary between 20 and 40 mg C m⁻³ and contribute an unknown positive bias to the results reported here. SOCCOM work commencing in 2017 will include this blank.

3. Data

All profiling float data used in this paper were downloaded from the SOCCOMViz web site. Two data files are available for each float. A raw data file that contains measurements processed with the laboratory calibrations for each parameter and a file that contains the quality-controlled and adjusted data. This later file contains the best estimates of each state variable. The processes used to produce this file are discussed below. The raw files were downloaded at <ftp://ftp.mbari.org/pub/SOCCOM/FloatVizData>. The quality-controlled files were obtained at <ftp://ftp.mbari.org/pub/SOCCOM/FloatVizData/QC/>. The full data set is archived with a digital object identifier (doi:10.6075/J09021PC), with the caveat that only data in that archive up to December 2016 were used in this paper. The hydrographic data from the deployment cruises were downloaded from the Carbon Dioxide Information and Analysis Center (CDIAC) at <http://cdiac.ornl.gov/oceans/SOCCOM/SOCCOM.html>. The Carbon and Climate Hydrographic Data Office (CCHDO) at <https://cchdo.ucsd.edu/search> under project name SOCCOM. The GLODAPv2 data set was also obtained from CDIAC at <http://cdiac.ornl.gov/oceans/GLODAPv2/>.

4. Results

SOCCOM profiling floats have returned several thousand vertical profiles for oxygen, nitrate, pH, and bio-optics (Table 3). Automated quality control has been applied to each of these profiles, followed by a periodic visual inspection. The automated QC consists primarily of a range check on the raw concentrations computed from each sensor (Table 3). These accepted minimum and maximum ranges for computed values follow Argo recommendations, or are tighter. Range checks tighter than Argo recommendations were applied where it appeared practical due to regional expectations. The visual inspection consists of a comparison of individual profiles with the aggregate data set produced by the float and nearby GLODAPv2 [*Olsen et al.*, 2016] or World Ocean Atlas 2013 [*Levitus et al.*, 2013] profiles. Large fractions of each sensor data pass these checks and are marked with a quality flag corresponding to good (Table 3). Data that do not pass checks are given a bad quality flag, but remain in the data set. This process may identify occasional single points that may result from processes such as particles in the optics of the nitrate sensor, intermittent fouling, as well as entire profiles if a sensor is failing. The nitrate and pH sensors have the lowest percentage of good data returned, but still near 90%. In both cases, the bulk of the bad data results from failing sensors. Nitrate sensor failures have primarily occurred due to biofouling, but a solution described below has been implemented that appears to mitigate this problem. pH sensors fail through three separate mechanisms

Table 3. Total Number of SOCCOM Float Profiles Through December 2016 and the Number Marked Good After Quality Control^a

Parameter	N Profiles	N Good	% Success	Range Check (min, max)
Oxygen	2832	2831	100	−5, 450
Nitrate	2427	2202	91	−10, 55
pH	2355	2065	88	7.3, 8.5
Chlorophyll	2166	2165	100	−0.1, 50
Backscatter	2166	2165	100	−0.01, 0.1

^aThe minimum and maximum values for the range check is also shown.

identified from diagnostic data transmitted along with pH information. Solutions for two of the three failure mechanisms have been implemented in recent generations of sensors. We hope to see data returns for both of these systems well above 95% in succeeding years.

The raw data returned by each sensor must then be adjusted to produce improved concentration estimates. The data adjustment procedure for SOCCOM float sensor data is based on the premise that errors in sensor gain (multiplicative correction) or offset (additive correction) that are identified at any particular point on a vertical profile can be applied over the entire profile to obtain an adjusted profile that more closely represents conditions in the ocean. The corrections are determined using methods that are independent of the data obtained on the hydrographic profile that accompanies each float deployment. In the following sections, we discuss the methods used to identify and quantify sensor error. We then assess the accuracy of the sensor correction process by comparing the initial profiles for each sensor to measurements made by conventional methods on samples collected at the time floats were deployed. The long-term accuracy of these approaches is evaluated with crossover analyses to stations from the GLODAPv2 database that were made at locations near float profiles. These cross over analyses may occur at long times after the initial float deployment (up to 3 years) and long distances (thousands of km) from the initial station.

4.1. Oxygen

The fluorescence lifetime oxygen sensors have proven to be robust and essentially 100% of the data have passed our preliminary quality checks (Table 3). However, these sensors are known to suffer from inaccurate initial calibration [Körtzinger *et al.*, 2005; D'Asaro and McNeil, 2013; Johnson *et al.*, 2015] and they have a relatively slow response time [Bittig *et al.*, 2014]. Sensor calibration errors were treated entirely as an error in sensor gain with the corrected oxygen concentration ($O_{2\text{ corr}}$) obtained from the equation

$$O_{2\text{ corr}} = G \times O_{2\text{ raw}}, \quad (1)$$

where G is the gain correction and the raw oxygen concentration ($O_{2\text{ raw}}$) was calculated from the calibration coefficients supplied by the manufacturer. Nearly all of the floats equipped with Aanderaa oxygen sensors were programmed to make measurements in air each time the float surfaced. The gain values for these sensors were determined from the air oxygen measurements as described by Johnson *et al.* [2015]. A single gain value was used for each sensor, with no correction for possible sensor drift. The impacts of this decision are discussed below. The SBE63 sensors are installed in the pumped flow stream of the CTD and they are not exposed to air when the float surfaces, so they cannot make air oxygen measurements. The gain correction for these floats and a few APEX floats whose sensors did not make air oxygen measurements were, therefore, determined by comparing the surface percent oxygen saturation values with the World Ocean Atlas climatology, as described by Takeshita *et al.* [2013].

The initial accuracy of the corrected oxygen concentrations was assessed by comparing the oxygen data on the first profile with the oxygen concentrations determined by Winkler titrations in samples collected at a station before the floats were deployed, referred to as the deployment cast. These stations typically occur 18 h before the float surfaces to make its first profile. Deployment casts with Winkler titrations were available for 41 floats at the time this paper was written. Figure 3 shows the corrected oxygen concentrations observed on the first float profile versus the Winkler titration values. The slope of a Model II regression is 1.009 and at the midpoint of the data, the float sensor data are offset low of the 1:1 relationship with the Winkler titration data by $3.7 \mu\text{mol kg}^{-1}$, or about 1.5% (Table 4). This offset is largely created by a cluster of data points in regions of the highest vertical oxygen gradients with absolute slopes greater than $0.5 \mu\text{mol kg}^{-1} \text{m}^{-1}$. The slow sensor response in these high gradients can produce an underestimate of the correct oxygen concentration and the data fall below the 1:1 line in Figure 3. Removing these data points shifts the average offset of the sensor data to 1% of the Winkler oxygen value. It is likely that the initial oxygen concentrations for the float population as a whole, after correction with the air oxygen gain value, are accurate to about 1%, with the exception of data within steep gradients. Bittig and Körtzinger [2017] note that it is possible to correct the oxygen data for the slow sensor response if the sample times are known. As SOCCOM floats do record the needed timing information, it should be possible to further improve the initial accuracy and consistency of the data.

Within the overall population of gain corrected oxygen data, a few floats show systematically greater offsets of their results from the Winkler titration values. The air-corrected oxygen sensor data from the first

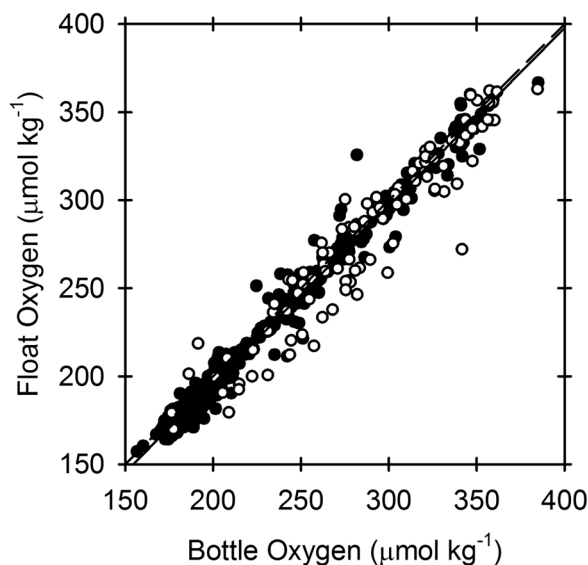


Figure 3. Air oxygen corrected profiling float oxygen concentrations on profile 1 versus concentrations measured by Winkler titration in samples collected on the deployment profile. Data were matched by depth. Open circles are float samples in regions with an absolute oxygen gradient larger than $0.5 \mu\text{mol kg}^{-1} \text{m}^{-1}$. Dashed line is 1:1 relationship and solid line is model II regression (Table 4).

six floats that were deployed on the P165 GO-SHIP cruise are systematically low of the deployment cast Winkler data by 10 to $15 \mu\text{mol kg}^{-1}$, which is about 3–5% of the Winkler reference value. These floats were equipped with oxygen sensors acquired at different times and they carried both Aanderaa 3830 and 4330 model optodes. There is no offset for floats deployed after the first six. Further investigation is required to understand the source of such offsets. The conclusions reported here for sensor performance must be considered to apply to the fleet as a whole, rather than individual floats.

The strong, linear correlation between the float sensor data and the bottle data confirms that a correction at a single point, atmospheric oxygen, can be applied to the entire profile. Neglecting measurements in the steepest oxygen gradients, the adjusted oxygen measurements appear to be accurate to within 1%. At this point in the SOCCOM program, no changes in oxygen sensor gain over

time have been made. The evidence for small amounts of oxygen sensor drift is discussed in section 4.4.

4.2. Nitrate

Both In Situ Ultraviolet Spectrophotometer (ISUS) and Submersible Ultraviolet Nitrate Analyzers (SUNA) optical nitrate sensors have been used in SOCCOM. These sensors detect nitrate directly from the UV absorption spectrum of the nitrate ion [Johnson and Coletti, 2002]. At the time this paper was submitted, 54 nitrate sensors have been deployed and the QC process initialized. Ninety-one percent of the expected data have been returned (Table 3). Two sensors failed due to electronic malfunctions. In addition, three of the first ten ISUS sensors suffered a rapid decrease in light throughput. We suspect that the loss of light transmission resulted from fouling due to the presence of *Phaeocystis antarctica*. *Phaeocystis* sp. is known to produce gelatinous aggregates that may foul sampling gear, including optics [MacKenzie et al., 2002]. The loss of light transmission was reversed over winter and then recurred during the subsequent spring bloom, indicating that the process was not failed optics. Organics must have built up on the optics and then been slowly lost during the winter, low-productivity season. The optical cells of the instruments with decreased light throughput were in the flow stream of the CTD pump. We subsequently removed the nitrate sensor optics from the pumped stream of the CTD on the presumption that exposing the optics to seawater and wave action at the surface would minimize this source of fouling. Since then only 2 of 44 nitrate sensors have lost optical throughput (4.5%).

Adjustment of the nitrate concentration determined from sensor data is based on the assumption that a correction determined at any one depth is a constant offset over the entire profile [Johnson et al., 2013]. Comparison of uncorrected nitrate sensor data on the first profile with samples collected from the CTD/

Table 4. Model II Regression Parameters for a Comparison of Corrected Sensor Data Flagged As Good Quality to Measurements in Bottle Samples Collected at the Time of Deployment^a

Parameter	Slope \pm 1 SD	SD	Bot.-Flt at Midrange	N
Oxygen	1.009 ± 0.005	8 (6)	3.7	798
Nitrate	1.009 ± 0.004	0.8	-0.1	581
pH	1.012 ± 0.010	0.015	0.006	429

^aUnequal values of N for each parameter result from different discrete sampling rates, lags in availability of sample data, and some sensor failures. SD value in parentheses results after removing data in high oxygen gradients.

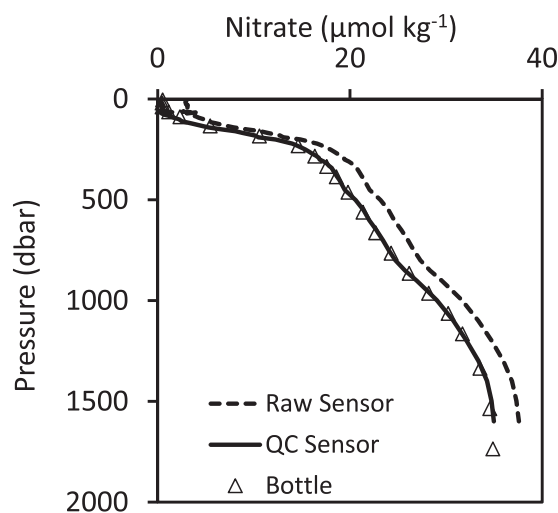


Figure 4. Raw and QC-corrected sensor nitrate on profile 1 from float 5904395/9254 (WMO number/UW serial number) and nitrate measured on board ship from a profile at the deployment site. A constant offset of $2.6 \mu\text{mol kg}^{-1}$ has been applied to the raw data to produce the QC data.

use with the MLR. The temperature and salinity are real-time values reported by the float, as delayed mode corrections for these variables are generally not available in real time and the corrections are small for this purpose. Float nitrate concentrations were initially adjusted by adding the offset from the MLR at 1500 m to every point on a profile. Drift corrections were then added when it became apparent that the sensor data at 1500 m on subsequent profiles was systematically changing relative to the 1500 m MLR estimate for each profile. The number of adjustments was minimized to the smallest number possible, while still maintaining consistency to within about $0.5 \mu\text{mol kg}^{-1}$ between sensor data and the MLR equation. This process is modeled on the procedures used to adjust Argo salinity data [Owens and Wong, 2009]. As an independent check on the correction process, the adjusted nitrate concentrations were also compared to the predictions of the CANYON neural network based system [Sautède et al., 2017]. Mismatches between the MLR and CANYON estimates were generally less than $1 \mu\text{mol kg}^{-1}$.

The adjustments for float 5904469/9096 are listed in Table 5. Figure 5 shows the raw and adjusted sensor data, and the nitrate values computed from the MLR at 1500 m depth. There are four nodes where either new offsets or drifts are applied to the data. The net correction at each node (ΔN_j) is computed as

$$\Delta N_j = \Delta N_{j-1} + O_j + D_{j-1}(T_j - T_{j-1}) \quad (2)$$

using the offsets (O), drifts (D), and times (T) at each node, which are listed in Table 5. The net correction at each node is also listed in the table. The net correction for a profile at cycle i , past node j and before the next node, is computed relative to the adjustment at node j as

$$\Delta N_i = \Delta N_j + D_j(T_i - T_j). \quad (3)$$

The corrections for cycle 1 of float 5904469/9096 are large, likely because the nitrate sensor optics were not cleaned before deployment. We have since implemented a protocol for cleaning the optics with methanol before deployment and recent drift rates are more similar to those seen after node 3. These much lower

Table 5. Nitrate Adjustment Parameters for Float 5904469/9096

Node	Cycle	Date	Gain	Offset ($\mu\text{mol/kg}$)	Drift ($\mu\text{mol/kg/yr}$)	Net ($\mu\text{mol/kg}$)
1	1	11 Dec 14	1	1.9	0	1.90
2	2	21 Dec 14	1	-4.8	-7	-2.90
3	10	14 Mar 15	1	0	-1.5	-4.48
4	37	18 Dec 15	1	0	-0.5	-5.63

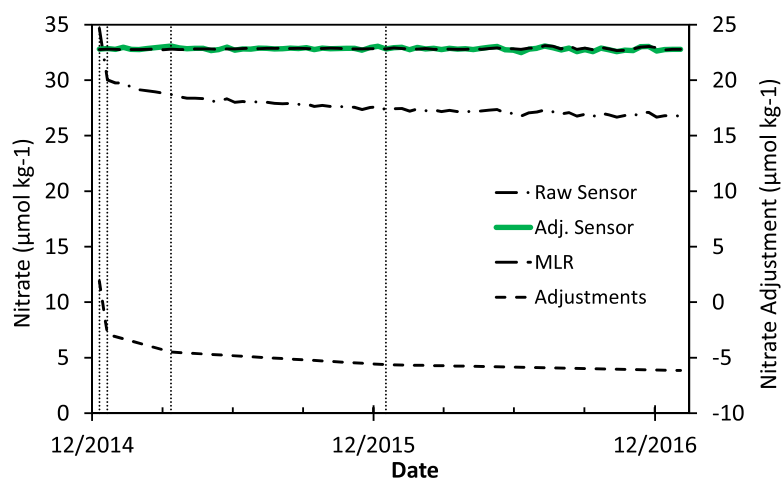


Figure 5. Nitrate sensor data at 1500 m depth for float 5904469/9096 and the predicted (MLR) nitrate concentrations. Dashed line shows the adjustments that are applied to the raw sensor data. Vertical dotted lines are locations of four nodes where changes in the adjustment parameters in Table 5 are applied.

drift rates generally fall in the range of $\pm 1.5 \mu\text{mol kg}^{-1} \text{y}^{-1}$. They likely result from aging of the UV lamp and the optics in the sensor.

The adjustment process is driven only by the match to the MLR equation and is relatively independent of bottle data from the hydrocast that precedes each float deployment, with the caveat that some bottle data from deployment cruises are in the GLODAPv2 data set used to develop the MLR [Williams *et al.*, 2016]. A fleet comparison of all of the nitrate sensor data from the first float profile with the station bottle data is shown in Figure 6. The slope of a regression line fitted to the data is not different from 1 and the offset of the sensor data from the bottle data is essentially zero (Table 4). The close match between sensor data and bottle data at all depths validates the approach used to correct the nitrate sensor data at the time the floats are deployed by adding only a constant offset to the entire profile.

The raw and adjusted nitrate concentrations may occasionally be reported as negative numbers when surface nitrate concentrations are near zero. It is somewhat traditional in oceanography to set the negative values to zero, as a negative concentration is physically impossible. However, the values returned by a sensor are estimates of concentration and these estimates may be negative when the real concentrations are near zero [Thompson, 1998]. Setting the negative, estimated concentrations to zero, a procedure termed “left censoring” of the data, has a detrimental impact on statistical assessments of data near zero concentration [Newman *et al.*, 1989]. We, therefore, retain the negative values in data sets that we report and mark the values with a quality flag indicating good data as these are valid estimates of nitrate concentration. The onus will be on users of the data to decide the appropriate procedure for utilizing these estimated values.

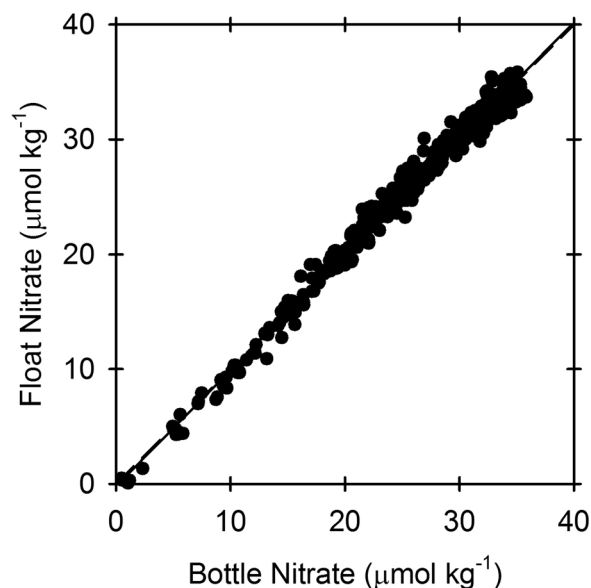


Figure 6. MLR-corrected nitrate concentrations from profile 1 versus deployment cast nitrate measured in the laboratory. Data were matched by depth. Dashed line is 1:1 relationship and solid line is the model II regression (Table 4).

4.3. pH

Deep-Sea DuraFET sensors [Johnson *et al.*, 2016a] were used to measure the in situ pH

Table 6. pH Sensor Calibration Media and Drift Rates in First 6 Months for Four Sets of Sensors^a

Year Class	Cal. Media	Drift/Year
2014	Tris	-0.083
2014/15	TT SW	-0.017
2015/16	TT SW	-0.011
2015/16	SW	0.003

^aThe calibration media was either Tris buffer in artificial seawater with no bromide (Tris), natural seawater from the MBARI test tank (TT SW), or raw seawater (SW).

pH to the MLR result were made by adding a constant offset to the reference potential of the sensor [Johnson *et al.*, 2016a], rather than to pH, directly. This was done because the available evidence suggests that sensor drift results from a reference potential change. Given a reference potential change, the shift in computed pH is slightly temperature dependent as the Nernst slope that transforms sensor potential to pH depends on temperature.

The initial set of sensors deployed for the SOCCOM project in early 2014 suffered from a relatively large initial drift rate during their first 6 months (Table 6). The sensors in this batch had been calibrated in Tris buffer in artificial seawater that did not contain bromide. The drift appeared to result because the AgCl reference sensor was not sufficiently conditioned to natural seawater. Exposure of the reference sensor to natural seawater shifts the reference potential due to the formation of a $\text{AgCl}_x\text{Br}_{1-x}$ solid solution. The next batch of sensors (2014/2015) was calibrated in seawater from the MBARI test tank, which is sterilized by ozonation. Unfortunately, one of the side reactions of ozonation is formation of bromate ion and the bromide levels are somewhat different than natural seawater. Drift rates in this batch of sensors were lower, but still relatively high. Subsequent batches of sensors were pretreated in a flowing raw seawater tank for several weeks before calibration of the reference potential and now have pH drift rates typically less than 0.01 year^{-1} .

To compensate for sensor drift, the reference potential of the pH sensors was corrected so that pH at 1500 m matched the estimates from the MLR equation [Williams *et al.*, 2016]. As for nitrate, a minimum number of nodes were used to make corrections that keep the sensor data within about 0.005 of the MLR estimate. Figure 7 shows the fleet comparison of pH sensor data on profile 2 after adjustment of the reference potential with the bottle data collected at the deployment station. The pH values from bottle samples measured in the

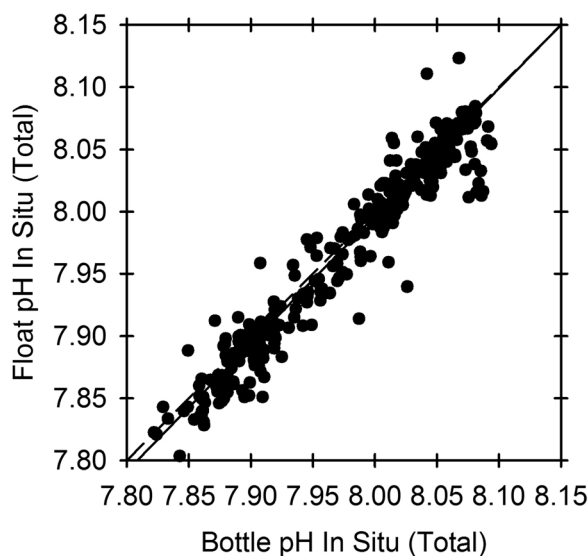


Figure 7. MLR-corrected pH from profile 2 versus deployment cast pH measured in the laboratory. Data were matched by depth. Dashed line is 1:1 relationship and solid line is model II regression (Table 4).

value on each float profile. The sensor reference potential, temperature coefficient, and pressure coefficient, which are needed to compute the in situ pH, were determined in the laboratory as described by Johnson *et al.* [2016a].

The pH data were corrected for offsets and drifts over time by a process similar to that used for nitrate. The MLR equations used to estimate pH at 1500 m are described in Williams *et al.* [2016].

The adjustments necessary to match the sensor

laboratory were converted to in situ conditions using the CO2Sys software [van Heuven *et al.*, 2011] and an estimate of the alkalinity [Carter *et al.*, 2016]. The equilibrium constants from Lueker *et al.* [2000], Dickson [1990], and Perez and Fraga [1987] were used in the calculations. We have chosen to use the pH sensor data from the second float profile to construct this plot because of the relatively large initial drifts caused by the lack of conditioning in some of the pH sensors. The slope of a model II regression through the data is again indistinguishable from 1 (Table 4). The scatter about the regression line is 0.017 in pH and the mean pH offset is 0.005. Examination of the residuals shows that the largest values are all in steep gradients and appear to result from processes such as internal waves that create mismatches in water properties at a given depth over the time between the hydrographic cast and the second float profile (up to 10 days).

4.4. Crossover Comparisons to GLODAPv2

The long-term consistency of the chemical sensor data was assessed by comparing the quality controlled and adjusted sensor results to the GLODAPv2 data set [Olsen *et al.*, 2016] for 56 of the SOCCOM floats which have undergone the QC process. If a float surfaced within 20 km of a profile in the GLODAPv2 database, the sensor data were matched to the values in the GLODAPv2 profile by a linear interpolation of the sensor values on depth. These crossover comparisons were made for all float data from the surface to the maximum depth reached by the float (Figure 8, left), and only for observations below 300 dbar to minimize seasonal variability (Figure 8, right). The comparisons between float and GLODAPv2 data were made on the basis of depth, to avoid problems matching densities in deep mixed layers. No selection was made on the basis of time, as the GLODAPv2 data set is heavily biased to summer months, as are all Southern Ocean ship-based data sets (Figure 1). Selecting on time greatly reduces the number of comparisons. Since our primary assessment is based on data below 300 m (Figure 8, right), where there should be little or no seasonal cycle, we report only the comparisons without time.

Table 7 summarizes the results of the crossover analyses using only data from below 300 m, which will minimize seasonal variability. The scatter of the measurements about the regression lines is larger than for the comparisons to the measurements made at the deployment stations (Table 4). The ratios of the standard deviations in Table 7 are 9:1.8:12 C:N:O, where a standard deviation of 0.023 in pH would correspond to a standard deviation of $9 \mu\text{mol kg}^{-1}$ in dissolved inorganic carbon at typical Southern Ocean alkalinity values. These ratios scale to 106:21:141, which is very close to the modified Redfield ratio of 106:16:150 [Anderson, 1995]. It is very likely that the scatter in Figure 8 results, primarily, from ocean variability that produces linked shifts in the distributions of pH, nitrate, and oxygen, rather than changes in sensor performance that fortuitously co-occur at near Redfield proportions.

The slopes of model II regression equations fitted to the oxygen and nitrate crossover data below 300 m are very close to 1. The mean difference for oxygen from GLODAPv2 minus the corresponding float value is $3 \pm 11 \mu\text{mol kg}^{-1}$ for depths below 300 m, where seasonal differences should be minimized (Table 7). The mean difference in GLODAPv2 minus sensor is similar to that observed at the time the sensors were deployed and the standard deviation of the data from the regression line is only marginally larger (Table 4). The offset of the sensor nitrate data from GLODAPv2 measurements near the middle of the concentration range is $-0.5 \mu\text{mol kg}^{-1}$. There is no evidence for a large degradation in oxygen or nitrate sensor performance as the floats age.

The slope of the pH sensor data versus the GLODAPv2 data at the crossover stations is significantly lower than 1 and the offset from the GLODAPv2 data (0.031 near pH 8.05) is relatively large and increases towards shallow depths (higher pH). This stands in contrast to the comparison with data collected at the float deployment (Table 4), where the slope is one and the offset is small. We do not believe that the low slope and large offset results from a degradation of sensor performance. The mean age of the pH data at the crossover stations that we have obtained from GLODAPv2 is 15 years. Acidification rates near $-0.0022 \text{ pH yr}^{-1}$ in Southern Ocean surface waters [Williams *et al.*, 2015] would produce mean biases of 0.033, similar to the offset observed here in near surface waters. The lowest pH values correspond to greater depths, where acidification signals are weaker. Offsets for sensor pH measurements near 1000 m are about 0.01 in pH, consistent with observed acidification rates in deep, Southern Ocean waters [Ríos *et al.*, 2015]. The slope of 0.93 for sensor pH data versus GLODAPv2 (Table 7) then results because the lowest pH values observed by the floats have been shifted the least by acidification and the highest values near the surface have been shifted the most.

4.5. Oxygen Sensor Gain Changes

The optode oxygen sensors used in SOCCOM appear to generally have good stability when deployed in the ocean. The oxygen data reported by the SOCCOM floats have, therefore, been corrected using a constant sensor gain. This results in a sensor with accuracy near 1% for the initial, surface ocean oxygen concentrations. The gain values for many floats do show a statistically significant change in time, as we have reported previously [Johnson *et al.*, 2015]. These changes are both positive and negative and, for a large number of floats, tend to average near zero. Optode oxygen sensor drift is generally only towards higher gain in time (decreased response to oxygen) [D'Asaro and McNeil, 2013]. As a result, we attributed the observed, significant changes in gain to other, unidentified factors [Johnson *et al.*, 2015]. However, there is some evidence that oxygen

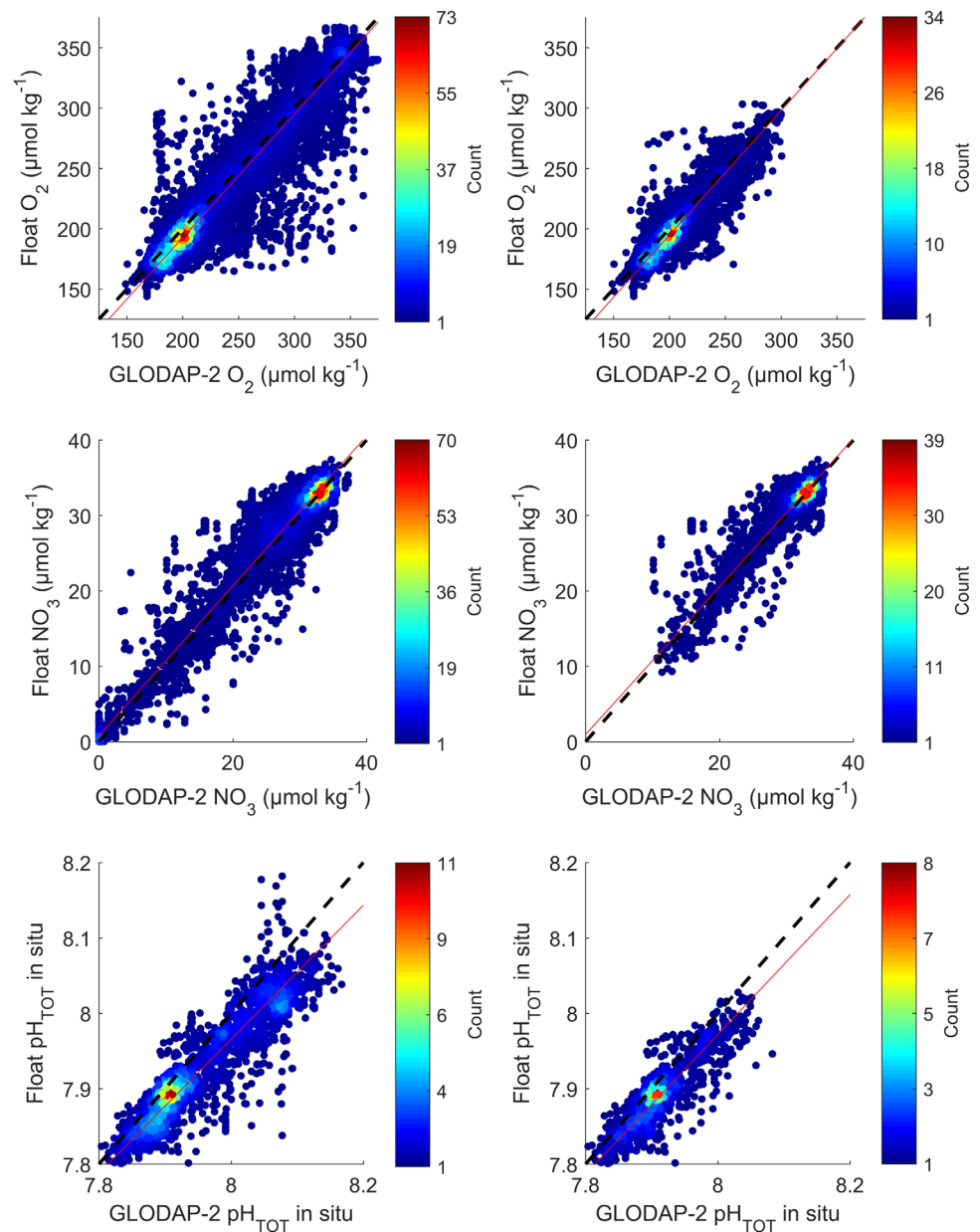


Figure 8. Comparison of float oxygen, nitrate, and pH data to GLODAPv2 measurements when a float profile occurs within 20 km of a GLODAPv2 profile. No selection was made based on time of year. Left figures show all comparisons from surface to maximum depth of a float profile. Right figures show only data from below 300 m depth. Dashed line is the 1:1 relationship and red line is a model II regression. Color scale shows number of data points at each grid point after dividing each axis by 200 units.

sensor drift rates are small, but not zero, when deployed in the ocean [Bushinsky et al., 2016; Bittig and Körtzinger, 2017]. We have, therefore, revisited the question of changes in sensor gain over time.

The observed oxygen sensor gain changes are shown in Figure 9. In a few cases, these changes are relatively large, equivalent to a 1% change in gain per year. The average is near zero and in most cases it

Table 7. Model II Regression of Float Versus GLODAP Data From Below 300 m Depth

Parameter	Slope	SD	GLDP-Fit at Midrange	N
Oxygen ($\mu\text{mol kg}^{-1}$)	1.028 ± 0.006	12	3.2	6246
Nitrate ($\mu\text{mol kg}^{-1}$)	0.983 ± 0.006	1.8	-0.5	4767
pH	0.93 ± 0.01	0.023	0.024	1361

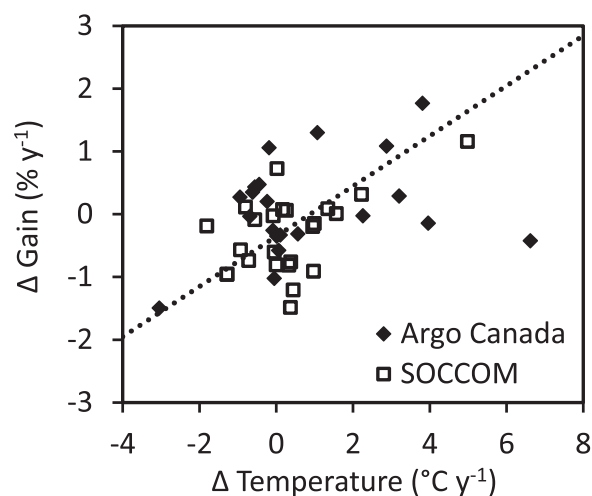


Figure 9. Changes in oxygen sensor gain per time are plotted versus the change in surface water temperature per time seen by the float. The slope of a model II regression ($0.40 \pm 0.05\%/^{\circ}\text{C}$ (1 SD, $N = 45$) is significant ($p < 0.005$).

is supported indirectly by the results of *Bushinsky et al.* [2016]. They deployed profiling floats with paired oxygen sensors. The temporal drifts of the complete oxygen data set from each sensor on a float are nearly identical, indicating that they are driven by an environmental factor that impacts both sensors equally. Temperature variations would be such an environmental factor. However, the R^2 value (Figure 9) is only 0.2, indicating that temperature variations account for only 20% of the gain change.

At this point in time, we have not corrected the oxygen data for this apparent temperature coefficient of the sensor. Pending further analysis of the float oxygen sensor data, we may implement an additional temperature correction, beyond that recommended by the manufacturer. However, there still appear to be significant variations in sensor gain over time that are not corrected by temperature alone.

4.6. Bio-Optical Sensors

The bio-optical sensors have shown high reliability (Table 3). Very rarely, a profile is marked bad because it appears that a large aggregate has been trapped on the sensor face. To check for sensor drift we looked at the signal at ~ 1000 m and found them to vary by only 2–3 digital counts in a range of 4096 (except for a few spikes) within the lifetime of a float. This variability is close to the sensitivity limit of the instruments (~ 1.4 counts for fluorescence and ~ 1.8 counts for backscattering). This indicates no change in the dark performance of the sensor. *Haëntjens et al.* [2017] have compared the bio-optical measurements near the surface with satellite observations and find no evidence of sensor drift. Here we briefly summarize the bio-optical products.

4.6.1. Optical Backscatter Sensor

A review of the optical backscattering sensor principles and performance, including WET Labs sensors, was recently published [*Sullivan et al.*, 2013]. We obtain the volume scattering function β from the sensor raw signal using the manufacturer's calibration

$$\beta(\theta) = \text{slope} \times (\text{signal} - \text{dark}), \quad (4)$$

where θ is the scattering angle (142° and 150° for FLBB and MCOMS, respectively, all at 700 nm). The manufacturer dark counts are used unless a predeployment dark measurement, determined with the sensor on the float, is available. The backscattering coefficient of particles b_{bp} is determined as

$$\beta_p(\theta) = \beta(\theta) - \beta_{sw}(\theta), \quad (5)$$

$$b_{bp} = 2 \times \pi \times \chi_p(\theta) \times \beta_p(\theta), \quad (6)$$

where $\beta_{sw}(\theta)$ is the volume scattering function of sea water using local temperature and salinity [*Zhang et al.*, 2009] and $\chi_p(\theta)$, with a value near 1.1, is the particulate conversion coefficient from *Sullivan et al.* [2013].

amounts to a few tenths percent per year. Not all of these changes in gain appear to result from drift of the sensor response itself. The rate of change in gain for all SOCCOM sensors deployed for more than two years, as well as the Argo Canada fleet analyzed previously [*Johnson et al.*, 2015], is significantly correlated with the rate of change in surface water temperature seen by the float (Figure 9). Floats drifting towards warmer regions see an increase in sensor gain over time (lower response to oxygen), while floats drifting to colder temperatures see a decrease in sensor gain (greater response to oxygen). The mean rate of change in gain for all floats is $-0.1\% \text{ yr}^{-1}$. This suggests that some of the gain changes are due to an uncompensated temperature coefficient in the sensor, perhaps related to the transient state that results when floats emerge from the ocean. This conclusion

Table 8. Regressions Between the Float Measurements of Chl *a* (mg m⁻³) or POC (mg m⁻³) and Discrete Samples Analysis (HPLC and POC)^a

Relationship	N	R ²	RMSD	RMSRD
$chl_{a,HPLC} = 0.15 (\pm 0.017) \times chl_{a,float}$	73	0.77	0.20	0.48
$chl_{a,HPLC} = 0.213 (\pm 0.016) \times chl_{a,float}^{0.714 (\pm 0.242)}$	73	0.80	0.12	0.37
$POC = 3.12 \times 10^4 (\pm 2.47 \times 10^3) \times b_{bp}(700) + 3.04 (\pm 6.78)$	67	0.76	35	0.47
$POC = 9.776 \times 10^4 (\pm 1.90 \times 10^4) \times b_{bp}(700)^{1.166 (\pm 0.173)}$	67	0.88	40	0.59

^aRMSD is root mean square deviation from the regression line and RMSRD is the root mean squared relative deviation from the regression line.

The concentration of POC was then estimated empirically from the b_{bp} sensor data. This POC estimate is reported in the data file with the quality controlled and adjusted data. POC concentrations measured from upper ocean water samples collected at the float deployment stations were regressed against b_{bp} measurements from the first profile of each float. The $b_{bp}(700)$ (b_{bp} at 700 nm) from the floats were averaged in the 5 m around the depth at which water samples were taken to minimize effects of spikes in the backscatter data, which integrates a much smaller volume than the water samples. The regression equation (Table 8 and Figure 10) is consistent with observations reported in the literature [Stramski et al., 1999, 2008; Loisel et al., 2001; Cetinic et al., 2012]. This equation was used to predict POC. The RMS deviation about the regression line corresponds to an uncertainty in POC of 35 mg m⁻³ (3 mmol C m⁻³), similar to the variability seen in other studies using similar sensors [Cetinic et al., 2012]. This uncertainty corresponds to the accuracy expected for a POC estimate. The relationship between POC and $b_{bp}(700)$ was derived for surface samples and it may be biased at depth below the MLD or euphotic zone. However, vertically resolved changes in the POC to $b_{bp}(700)$ ratio observed in other studies are on the order of 20% [Cetinic et al., 2012], similar to the error found above. Thus, an overall error for estimated POC might be the larger of 35 mg m⁻³ or 20%. Note that the zero intercept is not significantly different from zero, which is consistent with no significant bias during sample filtration arising from processes such as adsorption of dissolved organic compounds.

4.6.2. Chlorophyll a Fluorescence

The concentration of chl *a* (mg m⁻³) was initially estimated from the fluorescence signal using the linear calibration slope provided by the manufacturer

$$[chl]_{Raw} = slope \times (signal - dark). \tag{7}$$

In this calculation, the dark signal was determined with the sensor mounted on the float. These values are reported in the raw data files.

The raw chlorophyll concentrations determined from chlorophyll fluorescence suffer from two major deficiencies. Phytoplankton regulate the absorption and utilization of light energy, including energy received from the fluorometer. This photo-protection mechanism, known as nonphotochemical quenching (NPQ),

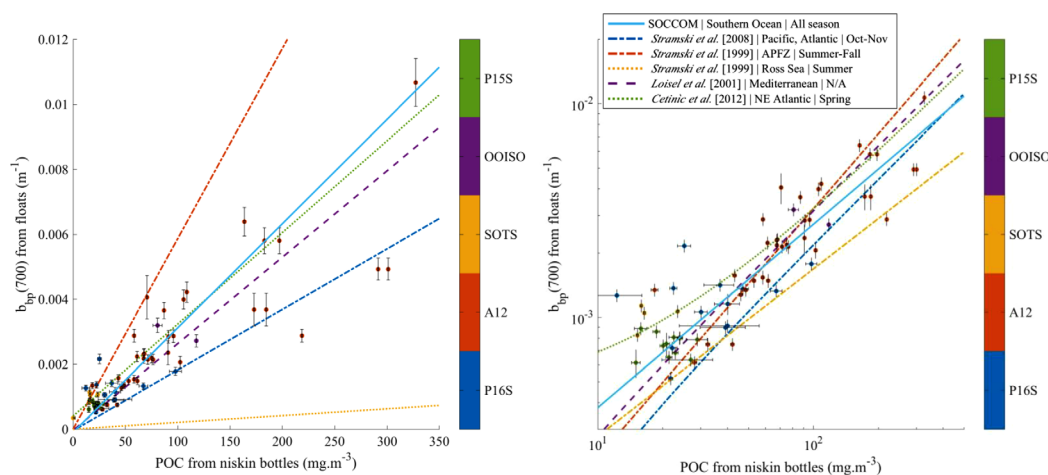


Figure 10. Relationship between POC (from discrete samples taken in the upper 100 m during float deployment) and $b_{bp}(700)$ on the first float profile on linear scales (left) and log scales (right). Equations reported in other studies are shown as dashed lines.

induces a large decrease in the fluorescence to chlorophyll ratio near the sea surface in daytime [Kolber and Falkowski, 1993; Muller *et al.*, 2001]. Several methods to correct for this bias exist and have been applied as described below. In addition, it has been understood for decades that the relationship between chlorophyll fluorescence and chlorophyll concentration is variable due to changes in phytoplankton physiology [Cullen, 1982]. One consequence of this can be significant biases between the estimate of chlorophyll concentration determined from the manufacturer's calibration equation and concentrations that are determined by HPLC even in the absence of NPQ [Roesler *et al.*, 2017]. As a first-order correction for this error, an empirical calibration was determined by comparing NPQ corrected $[chl a]_{Raw}$ to HPLC measurements. Both of these corrections are applied in the quality-controlled data file for each float as described below.

A comparison of NPQ corrected raw chlorophyll values to chlorophyll concentrations measured in the Southern Ocean has a linear slope of 6.4 (Figure 11a and Table 8). The raw chlorophyll sensor values thus appear too high by a factor over 6 in the Southern Ocean. This factor of 6 difference in HPLC chlorophyll and the raw sensors values is not an artifact of the time offset between sample collection and the first profile, as it persists at all time scales available for comparisons (data not shown). Roesler *et al.* [2017] recently assessed this issue more generally for WET Labs ECO fluorescence sensors. They concluded that the original calibration, which the manufacturer has maintained through time using artificial standards, has a global mean bias that results in chlorophyll sensor values too high by a factor of 2. Further, they find a gain correction in the Southern Ocean with floats other than those described here that is similar to the sixfold bias shown in Figure 11a. This difference must reflect regional influences of phytoplankton physiology. Roesler *et al.* [2017] recommend that the raw chl *a* values obtained with WET Labs ECO FLBB sensors be corrected by a factor of 2, which will produce a global set of data with a relatively small bias compared to global average HPLC values. We have applied this factor of 2 reduction to the adjusted chlorophyll data in our quality controlled data set. This would provide consistency with an adjusted global data set generated by FLBB sensors when there is no further calibration information. The meta data for this variable is accompanied by the recommended statement, "The community-established calibration bias of 2 for the WET Labs ECO-series fluorometer was applied to these in situ fluorometric chlorophyll values" [Roesler *et al.*, 2017].

Note that these twofold corrected chlorophyll values were not corrected for NPQ. Further, the large regional bias seen in the Southern Ocean chlorophyll fluorescence data is not fully compensated by a twofold correction. To produce a chlorophyll data set with a closer fidelity to Southern Ocean chlorophyll, a second chlorophyll product was included in the quality controlled data set. The raw chlorophyll concentration was corrected for NPQ effects and a gain correction of 6.4 was applied to the data set to bring our data into agreement with the HPLC values collected on the deployment casts. To determine if a profile requires a

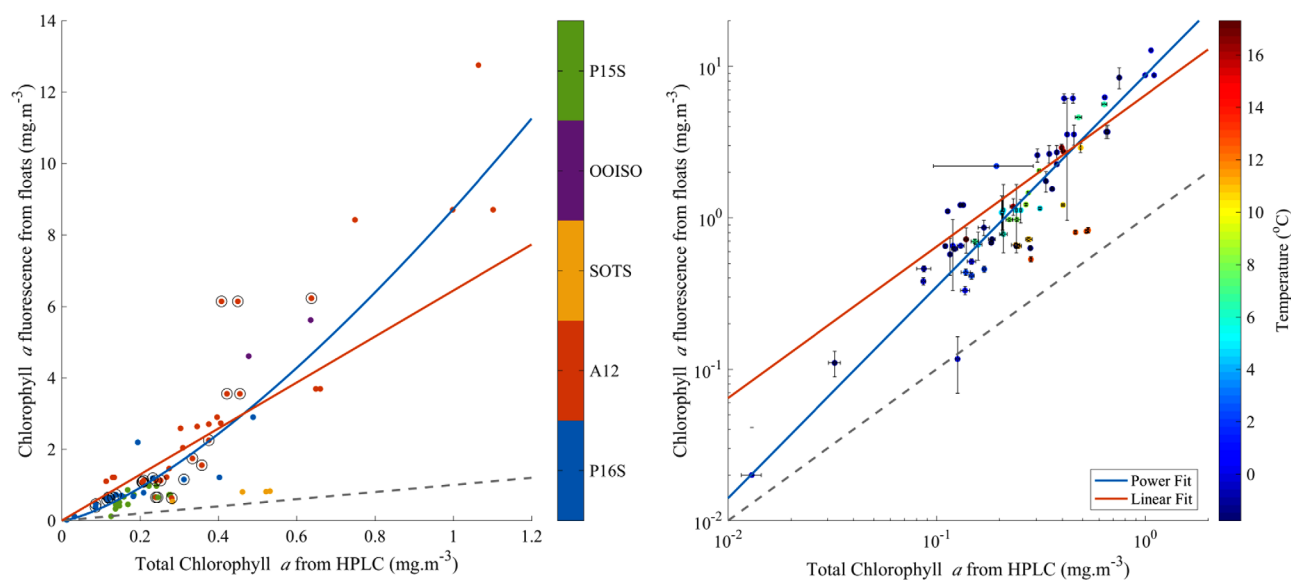


Figure 11. Relationship between total chlorophyll *a* (from HPLC) and chl *a* fluorescence (from floats) adjusted for darks and corrected for NPQ on a linear scale (left) and log/log scale (right). The red line is a linear fit with slope 6.4 (Table 8), the blue line is a power law fit (Table 8), and the 1:1 relationship is the dashed gray line.

correction for NPQ, the sun elevation angle was determined [Reda and Andreas, 2004]. The $[chl a]_{\text{Raw}}$ was corrected for NPQ if the sun elevation was greater than 5° . Corrections for NPQ were made using the average of two methods. Sackmann *et al.* [2008] uses the backscattering channel as a guide to extrapolate chlorophyll fluorescence to the surface. Xing *et al.* [2012] assumes a constant concentration of $[chl a]_{\text{Raw}}$ above the highest value found near the mixed layer depth (MLD). The MLD was estimated with a fixed density threshold criterion of 0.005 kg m^{-3} . In addition, the sensor dark signal for these calculations was determined following the procedures outlined by Xing *et al.* [2017] for a sensor without an FDOM channel. The dark signal was taken as the median of the minimum signal from ten profiles and this was used on all profiles. This essentially sets deep chlorophyll concentration to a value near zero.

The scatter of the corrected data chlorophyll values about the linear regression in Figure 11 is 0.2 and 0.12 mg m^{-3} for the power law fit. These would be reasonable estimates of chlorophyll uncertainty if one is confident that the population sampled on a new float profile has the same photo-physiological properties as that of the populations used to create Figure 11. However, the linear slope correction to the raw chlorophyll concentration estimates may vary from values near 2 in much of the ocean [Roesler *et al.*, 2017] to values near 6 in the Southern Ocean (Figure 11). It is also possible that the linear slope correction may vary in time [Xing *et al.*, 2011]. If one does not know, a priori, which factor to apply, the uncertainty in estimated chlorophyll can be larger than stated above. The chlorophyll values reported in the SOCCOM program have been validated through matchups with satellite estimates throughout the Southern Ocean and have been found to be consistent [Haëntjens *et al.*, 2017], which suggests that the linear slope correction is relatively constant. However, we caution that the corrected chlorophyll values, although consistent with our best understanding of Southern Ocean conditions, may carry additional uncertainty. If a robust estimate of biomass is required, we recommend using the POC concentration estimated from backscatter. The addition of downwelling irradiance sensors on profiling floats can help remove much of the additional uncertainty in estimates of chlorophyll concentration [Xing *et al.*, 2011] and this is being pursued.

5. Conclusions

Addressing the major questions in ocean biogeochemistry will require observing systems that operate year around throughout all the major ocean basins. Such systems will depend on autonomous chemical sensors. It is incumbent on the community to understand both the strengths and limitations of these systems as we develop new methods of ocean observing. It is clear from the work reported here that the current generation of chemical sensors are capable of generating high-quality products, but only if sufficient care is applied to compensate for limitations in the raw observations. The early evolution of oxygen sensor performance on profiling floats makes it clear that it is probably unreasonable to simply deploy sensors and expect high-quality data without additional effort at calibration and validation. However, it is also clear, both from the evolution of the quality of oxygen sensor data [Körtzinger *et al.*, 2005; Bittig and Körtzinger, 2015; Johnson *et al.*, 2015; Bushinsky *et al.*, 2016] and, more recently, pH data (Table 6) that sensors and our knowledge of their operation are improving. Independent efforts to validate bio-optical measurements at the global scale [Roesler *et al.*, 2017] are achieving similar results. Global scale, autonomous sensor networks are feasible.

The statistical comparison of the sensor output to the bottle samples collected near the time of the first float profile represent an upper limit on the initial accuracy of the sensors. The float profiles and the hydrocasts are never in exactly the same location or time, as the float does not surface until 18 h after it is deployed and the last activity on station is typically deployment of the float to ensure there is no chance of the ship running over a float. With that as a caveat, we note that the fleet average oxygen concentrations have a bias of $3 \mu\text{mol kg}^{-1}$, there is no significant bias for nitrate, and pH has a 0.006 bias (Table 4). Long-term experience with the nitrate sensor suggests that a more reasonable limit for initial accuracy is $0.5 \mu\text{mol kg}^{-1}$. These metrics are consistent with other analyses of sensor performance. For example, Williams *et al.* [2016] performed a detailed error analysis of the pH sensor and concluded that 0.007 was a reasonable limit on the accuracy of corrected data. The standard deviations about the regression lines in Table 4 must contain a significant contribution from oceanographic variability and do not reflect sensor precision alone. This effect is apparent because the ratios of the standard deviations in Table 4 are relatively close to the Redfield Ratio, as they are in Table 7. The standard deviations are dominated by ocean variability, rather than sensor noise. Considering the contribution of ocean variability, reasonable upper limits for the accuracy of the

initial, fleet average oxygen concentration is 1% at near surface oxygen concentrations. One standard deviation for individual sensors from this accuracy specification would be an additional 1%. Similarly for nitrate, we conclude that the fleet average accuracy is within $0.5 \mu\text{mol kg}^{-1}$ of bottle samples and individual sensors may deviate from this with a standard deviation of $0.5 \mu\text{mol kg}^{-1}$. The fleet average pH values lie within 0.005 of the bottle samples and individual sensors may scatter by 0.007 (one SD) from this mean offset. If air oxygen calibrations are not available, as is the case for two of our floats with Aanderaa optodes and all of the SBE63 oxygen sensors, then oxygen accuracy is likely worse than the value noted above. Oxygen sensor calibrations using air oxygen and comparisons to WOA have been made [Johnson *et al.*, 2015] and these suggest that the oxygen on floats without air measurements are probably only reliable to 3%.

These figures represent the overall initial accuracy that can be achieved when care is applied to compensate for calibrations that may have shifted due to aging, contamination (e.g., dirty optics) or shock during transport. These metrics also apply as the average over a large number of sensors. As noted above for oxygen, frequently an individual sensor will show greater deviations when compared to shipboard data. Because of this, care should be exercised when examining data from individual floats, rather than large numbers of sensors where these errors are minimized.

It is also clear that there are long-term shifts in the calibration of these chemical sensors. Compensating for these shifts requires a carefully developed procedure. The correction methods developed for the chemical parameters oxygen, nitrate, and pH are essentially independent of the data collected on the hydrographic cast when sensors are deployed. The procedure for oxygen is an assessment of error in the air oxygen measurement. For nitrate and pH, it is an assessment of the difference from concentrations estimated with MLR equations at depths near 1500 m where the ocean has longer-term stability and little seasonal variability. The primary validation for these correction schemes is the comparison to the laboratory measurements made on samples collected near the time the float was deployed.

The corrections are validated over longer time periods by comparing the corrected data to estimations of neural network systems [Sauzède *et al.*, 2017] and observations in the GLODAPv2 data set. The accuracy of the sensor data for nitrate and pH should not degrade appreciably in time because the correction process is the same as that used to make the initial corrections that produce the favorable comparison to independent deployment profiles (Table 4). It does appear from the air oxygen observations that some sensors begin to deviate from their initial calibration over time. In part, this seems to be due to an uncompensated temperature coefficient, as noted above. We have not attempted to correct for this error at the present time. As a result, some of our sensors may accumulate oxygen errors on the order of 0.5% per year. However, the fleet average drift rate for oxygen remains close to zero. This is clearly an area where additional work must be done. It may be feasible to improve oxygen sensor accuracy into the tenths of a percent region with further improvements.

These shipboard measurements remain essential, in the short term, to validate correction schemes for floats in new regions or for new sensors. However, it is also possible to envision a future where a hydrographic cast need not be coupled to each float deployment. This does not, however, free a biogeochemical sensor network from shipboard sampling. The correction scheme for sensor data depends on having accurate estimates of deep chemical concentrations, where concentrations are relatively stable and can be predicted using interpolation methods (multiple linear regressions or neural networks) based on shipboard observations. It is also clear from the pH observations that, even in the deepest waters reached by our profiling floats, there are anthropogenic changes in chemical concentrations. The long-term success of a global chemical sensor observing system will depend on support from an ongoing, shipboard hydrographic program to produce a high-quality data set for deep waters at the global scale. The shipboard measurements should meet the specifications listed by Olsen *et al.* [2016, Table 2] (oxygen, 1%; nutrients, 2%; pH, 0.005). The adjusted float sensor data are close to these specifications. However, until the biogeochemical sensors can be demonstrated to have a similar initial accuracy and high stability, the profiling float measurements will remain dependent on a background of ship-based observations. This relationship is mutually beneficial, as the floats can then provide a perspective on seasonal changes that shipboard programs have not been able to achieve.

The bio-optical sensors for optical backscattering and chlorophyll fluorescence appear stable in time, in most cases. The empirical conversion factor determined for backscattering by particles to POC is consistent with factors determined in other regions of the ocean. The data-estimated POC data appear accurate to

within about $3 \mu\text{mol C kg}^{-1}$. However, the number of comparisons remains fairly limited and should be expanded to other regions. It is clear that large changes in the conversion factor for chlorophyll fluorescence to chlorophyll occur. Deployments of fluorimetric chlorophyll sensors will require continuous assessments of calibration accuracy, including in situ calibration using irradiance sensors [Xing *et al.*, 2012].

The metrics discussed here apply to sensor accuracy. Short-term sensor precision is typically much better. Over a single profile, oxygen and nitrate concentrations are precise (1 SD) to order of $0.1 \mu\text{mol kg}^{-1}$, which is based on variability of measurements in the mixed layer on a single profile. pH values are typically precise to 0.001. Such high precision can enable additional types of studies, but this precision should not be confused with sensor accuracy.

Finally, we note that the current correction scheme for sensors is conducted on a float by float basis. At some point in the future, when the global biogeochemical fleet of profiling floats reaches a critical size, consideration should be given to performing a systematic optimization of the entire fleet data set, similar to the optimization described in Olsen *et al.* [2016] for the GLODAPv2 data set. This would likely produce an extremely homogeneous data set with spatial and temporal resolution that would greatly improve our understanding of ocean biogeochemistry and serve as an improved tool to constrain ocean models.

Acknowledgments

Float data were collected and made freely available by the Southern Ocean Carbon and Climate Observations and Modeling (SOCCOM) Project funded by National Science Foundation, Division of Polar Programs (NSF PLR-1425989), supplemented by NOAA grant NA15OAR4320063 to S.R. and from NASA grant NNX14AP49G to E.B. Temperature and salinity data from SOCCOM floats are available in near-real time from Argo at <http://doi.org/10.17882/42182> and were made freely available by the International Argo Program and the national programs that contribute to it. Logistical support for this project in Antarctica was provided by the U.S. National Science Foundation through the U.S. Antarctic Program. Work at MBARI was also supported by the David and Lucile Packard Foundation. We thank all of the people involved in the construction, calibration, and deployment of SOCCOM floats and sensors and the crews of the ships that carried them to sea. Scientific Committee on Oceanic Research Working Group 142 contributed significantly to our understanding of oxygen sensor calibration. All data used in this paper are available at the locations specified in section 3.

References

- Anderson, L. A. (1995), On the hydrogen and oxygen content of marine phytoplankton, *Deep Sea Res., Part I*, 42(9), 1675–1680.
- Bakker, D. C. E., *et al.* (2016), A multi-decade record of high-quality $f\text{CO}_2$ data in version 3 of the surface ocean CO_2 atlas (SOCAT), *Earth Syst. Sci. Data*, 8, 297–323, doi:10.5194/essd-2016-15.
- Bednaršek, N., G. A. Tarling, D. C. E. Bakker, S. Fielding, E. M. Jones, H. J. Venables, P. Ward, A. Kuzirian, B. Lézé, R. A. Feely, and E. J. Murphy (2012), Extensive dissolution of live pteropods in the Southern Ocean, *Nat. Geosci.*, 5, 881–885, doi:10.1038/NGEO1635.
- Biogeochemical-Argo Planning Group (2016), *The Scientific Rationale, Design and Implementation Plan for a Biogeochemical-Argo Float Array*, edited K. S. Johnson and H. Claustre, doi:10.13155/46601.
- Bittig, H. C., and A. Körtzinger (2015), Tackling oxygen optode drift: Near-surface and in-air oxygen optode measurements on a float provide an accurate in situ reference, *J. Atmos. Oceanic Technol.*, 32(8), 1536–1543, doi:10.1175/jtech-d-14-00162.1.
- Bittig, H. C., and A. Körtzinger (2017), Technical note: Update on response times, in-air measurements, and in situ drift for oxygen optodes on profiling platforms, *Ocean Sci.*, 13(1), 1–11.
- Bittig, H., B. Fiedler, R. Scholz, G. Krahnemann, and A. Körtzinger (2014), Time response of oxygen optodes on profiling platforms and its dependence on flow speed and temperature, *Limnol. Oceanogr. Methods*, 12, 617–636.
- Boss, E., D. Swift, L. Taylor, P. Brickley, R. Zaneveld, S. Riser, M. J. Perry, and P. G. Strutton (2008), Observations of pigment and particle distributions in the western North Atlantic from an autonomous float and ocean color satellite, *Limnol. Oceanogr.*, 53, 2112–2122, doi:10.4319/lo.2008.53.5\part\2.2112.
- Bushinsky, S. M., S. R. Emerson, S. C. Riser, and D. D. Swift (2016), Accurate oxygen measurements on modified Argo floats using in situ air calibrations, *Limnol. Oceanogr. Methods*, 14(8), 491–505, doi:10.1002/lom3.10107.
- Carter, B. R., N. L. Williams, A. R. Gray, and R. A. Feely (2016), Locally interpolated alkalinity regression for global alkalinity estimation, *Limnol. Oceanogr. Methods*, 14, 268–277, doi:10.1002/lom3.10087.
- Cetinic, I., M. J. Perry, N. T. Briggs, E. Kallin, E. A. D'Asaro, and C. M. Lee (2012), Particulate organic carbon and inherent optical properties during 2008 North Atlantic bloom experiment, *J. Geophys. Res. Oceans*, 117, C06028, doi:10.1029/2011JC007771.
- Cullen, J. J. (1982), The deep chlorophyll maximum: Comparing vertical profiles of chlorophyll *a*, *Can. J. Fish. Aquat. Sci.*, 39, 791–803.
- D'Asaro, E. A., and C. McNeil (2013), Calibration and stability of oxygen sensors on autonomous floats, *J. Atmos. Oceanic Technol.*, 30, 1896–1906, doi:10.1175/JTECH-D-12-00222.1.
- Dickson, A. G. (1990), Standard potential of the reaction: $\text{AgCl}(s) + 1/2 \text{H}_2(g) = \text{Ag}(s) + \text{HCl}(aq)$, and the standard acidity constant of the ion HSO_4 in synthetic sea water from 273.15 to 318.15 K, *J. Chem. Thermodyn.*, 22(2), 113–127, doi:10.1016/0021-9614(90)90074-Z.
- Dickson, A. G., C. L. Sabine, and J. R. Christian (Eds.) (2007), Guide to Best Practices for Ocean CO_2 Measurement, PICES Spec. Publ. 3, North Pac. Mar. Sci. Organ., Sidney, B. C., Canada.
- Frölicher, T. L., J. L. Sarmiento, D. J. Paynter, J. P. Dunne, J. P. Krasting, and M. Winton (2015), Dominance of the Southern Ocean in anthropogenic carbon and heat uptake in CMIP5 models, *J. Clim.*, 28, 862–886, doi:10.1175/JCLI-D-14-00117.1.
- Gardner, W. D., M. J. Richardson, C. A. Carlson, D. Hansell, and A. V. Mishonov (2003), Determining true particulate organic carbon: Bottles, pumps and methodologies, *Deep Sea Res., Part II*, 50, 655–674.
- Haëntjens, N., Boss, E. and Talley, L. D. (2017), Revisiting Ocean Color algorithms for chlorophyll *a* and particulate organic carbon in the Southern Ocean using biogeochemical floats, *J. Geophys. Res. Oceans*, doi:10.1002/2017JC012844.
- Hood, E. M., C. L. Sabine, and B. M. Sloyan (Eds.) (2010), The GO-SHIP repeat hydrography manual: A collection of expert reports and guidelines, *ICPO Publ. Ser. 134, IOCCP Rep. 14*, pp. 1–88, U. N. Educ. Sci. and Cult. Organ. Intergov. Oceanotr. Comm., Paris. [Available at <http://www.go-ship.org/HydroMan.html>.]
- Hooker, S. B., *et al.* (2005), The second SeaWiFS HPLC analysis round-Robin experiment (SeaHARRE-2), *NASA Tech. Memo.* 2005-212785, 112 pp., Goddard Space Flight Cent., Greenbelt, Md.
- Johnson, K. S., and L. J. Coletti (2002), In situ ultraviolet spectrophotometry for high resolution and long term monitoring of nitrate, bromide and bisulfide in the ocean, *Deep Sea Res., Part I*, 49, 1291–1305.
- Johnson, K. S., and H. Claustre (2016), Bringing biogeochemistry into the Argo age, *Eos*, 97, doi:10.1029/2016EO062427.
- Johnson, K. S., J. A. Needoba, S. C. Riser, and W. J. Showers (2007), Chemical sensor networks for the aquatic environment, *Chem. Rev.*, 107, 623–640, doi:10.1021/cr050354e.
- Johnson, K. S., L. Coletti, H. Jannasch, C. Sakamoto, D. Swift, and S. Riser (2013), Long-term nitrate measurements in the ocean using the in situ ultraviolet spectrophotometer: Sensor integration into the apex profiling float, *J. Atmos. Oceanic Technol.*, 30, 1854–1866, doi:10.1175/JTECH-D-12-00221.1.

- Johnson, K. S., J. N. Plant, S. C. Riser, and D. Gilbert (2015), Air oxygen calibration of oxygen optodes on a profiling float array, *J. Atmos. Oceanic Technol.*, *32*, 2160–2172, doi:10.1175/JTECH-D-15-0101.1.
- Johnson, K. S., H. W. Jannasch, L. J. Coletti, V. A. Elrod, T. R. Martz, Y. Takeshita, R. J. Carlson, and J. G. Connery (2016a), Deep-sea DuraFET: A pressure tolerant pH sensor designed for global sensor networks, *Anal. Chem.*, *88*, 3249–3256, doi:10.1021/acs.analchem.5b04653.
- Johnson, K. S., P. D. F. Orens, S. Romain, D. Fabrizio, S. Catherine, C. Hervé, and P. Antoine (2016b), Processing bio-Argo nitrate concentration at the DAC level, v1.0, IFREMER, France, doi:10.13155/46121.
- Kennicutt, M. C., and S. L. Chown (2014), Six priorities for Antarctic science, *Nature*, *512*, 23–25.
- Kolber, Z., and P. G. Falkowski (1993), Use of active fluorescence to estimate phyto-plankton photosynthesis in situ, *Limnol. Oceanogr.*, *38*(8), 1646–1665, doi:10.4319/lo.1993.38.8.1646.
- Körtzinger, A., J. Schimanski, U. Send, and D. Wallace (2004), The ocean takes a deep breath, *Science*, *306*(5700), 1337.
- Körtzinger, A., J. Schimanski, and U. Send (2005), High quality oxygen measurements from profiling floats: A promising new technique, *J. Atmos. Oceanic Technol.*, *22*, 302–308.
- Landschützer, P., N. Gruber, and D. C. E. Bakker (2016), Decadal variations and trends of the global ocean carbon sink, *Global Biogeochem. Cycles*, *30*, 1396–1417, doi:10.1002/2015GB005359.
- Lee, K. (2001), Global net community production estimated from the annual cycle of surface water total dissolved inorganic carbon, *Limnol. Oceanogr.*, *46*, 1287–1297, doi:10.4319/lo.2001.46.6.1287.
- Levitus, S., et al. (2013), The world ocean database, *Data Sci. J.*, *12*, 229–234, doi:10.2481/dsj.WDS-041.
- Liu, X., M. C. Patsavas, and R. H. Byrne (2011), Purification and characterization of meta-cresol purple for spectrophotometric seawater pH measurements, *Environ. Sci. Technol.*, *45*, 4862–4868, doi:10.1021/es200665d.
- Loisel, H., E. Bosc, D. Stramski, K. Oubelkheir, and P. Y. Deschamps (2001), Seasonal variability of the backscattering coefficient in the Mediterranean Sea based on Satellite SeaWiFS imagery, *Geophys. Res. Lett.*, *28*(22), 4203–4206, doi:10.1029/2001GL013863.
- Lueker, T. J., A. G. Dickson, and C. D. Keeling (2000), Ocean pCO₂ calculated from dissolved inorganic carbon, alkalinity, and equations for K₁ and K₂: Validation based on laboratory measurements of CO₂ in gas and seawater at equilibrium, *Mar. Chem.*, *70*(1–3), 105–119, doi:10.1016/S0304-4203(00)00022-0.
- MacCready, P., and P. Quay (2001), Biological export flux in the Southern Ocean estimated from a climatological nitrate budget, *Deep Sea Res., Part II*, *48*, 4299–4322, doi:10.1016/S0967-0645(01)00090-X.
- MacKenzie, L., I. Sims, V. Beuzenberg, and P. Gillespie (2002), Mass accumulation of mucilage caused by dinoflagellate polysaccharide exudates in Tasman Bay, New Zealand, *Harmful Algae*, *1*, 69–83.
- Majkut, J. D., B. R. Carter, T. L. Frölicher, C. O. Dufour, K. B. Rodgers, and J. L. Sarmiento (2014), An observing system simulation for Southern Ocean carbon dioxide uptake, *Philos. Trans. R. Soc. A*, *372*, doi:10.1098/rsta.2013.0046.
- McNeil, B. I., and R. J. Matear (2008), Southern Ocean acidification: A tipping point at 450-ppm atmospheric CO₂, *Proc. Natl. Acad. Sci. U. S. A.*, *105*, 18,860–18,864, doi:10.1073/pnas.0806318105.
- Muller, P., X. Li, and K. Niyogi (2001), Non-photochemical quenching. A response to excess Light energy, *Plant Physiol.*, *125*(4), 1558–1566, doi:10.1104/pp.125.4.1558.
- Munro, D., N. Lovenduski, B. Stephens, T. Newberger, K. Arrigo, T. Takahashi, P. Quay, J. Sprintall, N. Freeman, and C. Sweeney (2015), Estimates of net community production in the Southern Ocean determined from time series observations (2002–2011) of nutrients, dissolved inorganic carbon, and surface ocean pCO₂ in drake passage, *Deep Sea Res., Part II*, *114*, 49–63, doi:10.1016/j.dsr2.2014.12.014.
- Newman, M. C., P. M. Dixon, B. B. Looney, and J. E. Pinder III (1989), Estimating mean and variance for environmental samples with below detection limit observations, *J. Am. Water Resour. Assoc.*, *25*, 905–916.
- Olsen, A., et al. (2016), The Global Ocean Data Analysis Project version 2 (GLODAPv2)—An internally consistent data product for the world ocean, *Earth Syst. Sci. Data*, *8*, 297–323, doi:10.5194/essd-8-297-2016.
- Owens, W. B., and A. P. S. Wong (2009), An improved calibration method for the drift of the conductivity sensor on autonomous CTD profiling floats by theta-S climatology, *Deep Sea Res., Part I*, *56*(3), 450–457, doi:10.1016/j.dsr.2008.09.008.
- Pasqueron de Fommervault, O., et al. (2015), Seasonal variability of nutrient concentrations in the Mediterranean Sea: Contribution of Bio-Argo floats, *J. Geophys. Res. Oceans*, *120*, 8528–8550, doi:10.1002/2015JC011103.
- Perez, F. F., and F. Fraga (1987), Association constant of fluoride and hydrogen ions in seawater, *Mar. Chem.*, *21*(2), 161–168, doi:10.1016/0304-4203(87)90036-3.
- Reda, I., and A. Andreas (2004), Solar position algorithm for solar radiation applications, *Solar Energy*, *76*(5), 577–589, doi:10.1016/j.solener.2003.12.003.
- Ríos, A. F., L. Resplandy, M. I. García-Ibáñez, N. M. Fajar, A. Velo, X. A. Padin, R. Wanninkhof, R. Steinfeldt, G. Rosón, and F. F. Pérez (2015), Decadal acidification in the water masses of the Atlantic Ocean, *Proc. Natl. Acad. Sci. U. S. A.*, *112*(32), 9950–9955, doi:10.1073/pnas.1504613112.
- Roesler, C., et al. (2017), Recommendations for obtaining unbiased chlorophyll estimates from in situ chlorophyll fluorometers: A global analysis of WET Labs ECO sensors, *Limnol. Oceanogr. Methods*, *15*, 572–585, doi:10.1002/lom3.10185.
- Sackmann, B. S., M. J. Perry, and C. C. Eriksen (2008), Seaglider observations of variability in daytime fluorescence quenching of chlorophyll-a in Northeastern Pacific coastal waters, *Biogeosci. Discuss.*, *5*(4), 2839–2865, doi:10.5194/bgd-5-2839-2008.
- Sarmiento, J. L., N. Gruber, M. A. Brzezinski, and J. P. Dunne (2004), High latitude controls of thermocline nutrients and low latitude biological productivity, *Nature*, *427*, 56–60, doi:10.1038/nature02127.
- Sauzède, R., H. Claustre, O. Pasqueron de Fommervault, H. Bittig, J.-P. Gattuso, L. Legendre, and K. S. Johnson (2017), Global estimates of water column nutrients concentration and carbonate system parameters in the Ocean: A novel approach based on neural networks, *Front. Mar. Sci.*, *4*, 128, doi:10.3389/fmars.2017.00128.
- Schmechtig, C., P. Antoine, C. Hervé, D. Fabrizio, and B. Emmanuel (2015), Processing bio-Argo chlorophyll-a concentration at the DAC level, v1.0, IFREMER, France, doi:10.13155/39468.
- Schmechtig, C., A. Poteau, H. Claustre, F. D'Ortenzio, G. Dall'Olmo, and E. Boss (2016), Processing bio-Argo particle backscattering at the DAC level, v1.2, IFREMER, France, doi:10.13155/39459.
- Stramski, D., R. A. Reynolds, M. Kahru, and B. G. Mitchell (1999), Estimation of particulate organic carbon in the ocean from satellite remote sensing, *Science*, *285*(5425), 239–242, doi:10.1126/science.285.5425.239.
- Stramski, D., et al. (2008), Relationships between the surface concentration of particulate organic carbon and optical properties in the eastern South Pacific and eastern Atlantic Oceans, *Biogeosciences*, *5*(1), 171–201, doi:10.5194/bg-5-171-2008.
- Sullivan, J. M., M. S. Twardowski, J. Ronald, V. Zaneveld, and C. C. Moore (2013), *Light Scattering Reviews*, Springer Praxis Books, vol. 7, 567 pp., Springer, Berlin Heidelberg, doi:10.1007/978-3-642-10336-0.
- Takeshita, Y., T. R. Martz, K. S. Johnson, J. N. Plant, D. Gilbert, S. C. Riser, C. Neill, and B. Tilbrook (2013), A climatology-based quality control procedure for profiling float oxygen data, *J. Geophys. Res. Oceans*, *118*, 5640–5650, doi:10.1002/jgrc.20399.

- Takahashi, T., S. C. Sutherland, D. W. Chipman, J. G. Goddard, and C. Ho (2014), Climatological distributions of pH, pCO₂, total CO₂, alkalinity, and CaCO₃ saturation in the global surface ocean, and temporal changes at selected locations, *Mar. Chem.*, *164*, 95–125, doi:10.1016/j.marchem.2014.06.004.
- Talley, L. D., et al. (2016), Changes in ocean heat, carbon content, and ventilation: A review of the first decade of GO-SHIP global repeat hydrography, *Annu. Rev. Mar. Sci.*, *8*, 185–215, doi:10.1146/annurev-marine-052915-100829.
- Thierry, V., D. Gilbert, T. Kobayashi, C. Schmid, and S. Kanako (2016), Processing Argo oxygen data at the DAC level, v2.2, IFREMER, France, doi:10.13155/39795.
- Thompson, M. (1988), Do we really need detection limits?, *Analyst*, *123*, 405–407.
- Van Heukelem, L., and C. S. Thomas (2001), Computer-assisted high-performance liquid chromatography method development with applications to the isolation and analysis of phytoplankton pigments, *J. Chromatogr. A*, *910*(1), 31–49, doi:10.1016/S0378-4347(00)00603-4.
- van Heuven, S., D. Pierrot, J. W. B. Rae, E. Lewis, and D. Wallace (2011), MATLAB Program Developed for CO₂ System Calculations, ORNL/CDIAC-105b, Carbon Dioxide Inform. Anal. Cent., Oak Ridge Natl. Lab., U.S. Dep. of Energy, Oak Ridge, Tenn., doi:10.3334/CDIAC/otg.CO2.SYS_MATLAB_v1.1.
- Williams, N. L., R. A. Feely, C. L. Sabine, A. G. Dickson, J. H. Swift, L. D. Talley, and J. L. Russell (2015), Quantifying anthropogenic carbon inventory changes in the Pacific sector of the Southern Ocean, *Mar. Chem.*, *174*, 147–160, doi:10.1016/j.marchem.2015.06.015.
- Williams, N. L., L. W. Juranek, K. S. Johnson, R. A. Feely, S. C. Riser, L. D. Talley, J. L. Russell, J. L. Sarmiento, and R. Wanninkhof (2016), Empirical algorithms to estimate water column pH in the Southern Ocean, *Geophys. Res. Lett.*, *43*, 3415–3422, doi:10.1002/2016GL068539.
- Williams, N. L., et al. (2017), Calculating surface ocean pCO₂ from biogeochemical Argo floats equipped with pH: An uncertainty analysis, *Global Biogeochem. Cycles*, *31*, 591–604, doi:10.1002/2016GB005541.
- Wong, A. P. S., and S. C. Riser (2011), Profiling float observations of the upper ocean under sea ice off the Wilkes Land coast of Antarctic, *J. Phys. Oceanogr.*, *41*, 1102–1115.
- Xing, X., A. Morel, H. Claustre, D. Antoine, F. D'Ortenzio, A. Poteau, and A. Mignot (2011), Combined processing and mutual interpretation of radiometry and fluorimetry from autonomous profiling Bio-Argo floats: Chlorophyll a retrieval, *J. Geophys. Res.*, *116*, C06020, doi:10.1029/2010JC006899.
- Xing, X., H. Claustre, and S. Blain (2012), Quenching correction for in vivo chlorophyll fluorescence acquired by autonomous platforms: A case study with instrumented elephant seals in the Kerguelen region (Southern Ocean), *Limnol. Oceanogr.*, *10*, 483–495, doi:10.4319/lom.2012.10.483.
- Xing, X., H. Claustre, E. Boss, C. Roesler, E. Organelli, A. Poteau, M. Barbieux, and F. D'Ortenzio (2017), Correction of profiles of in-situ chlorophyll fluorometry for the contribution of fluorescence originating from non-algal matter, *Limnol. Oceanogr. Methods*, *15*, 80–93, doi:10.1002/lom3.10144.
- Zhang, X., L. Hu, and M.-X. He (2009), Scattering by pure seawater: Effect of salinity, *Opt. Express*, *17*(7), 5698–5710, doi:10.1364/OE.17.012685.